Journal of Materials Chemistry

Cite this: J. Mater. Chem., 2012, 22, 24139

www.rsc.org/materials

PAPER

Flexible lasers based on the microstructured single-crystalline ultrathin films

Hong-Hua Fang,[a] Ran Ding,[a] Shi-Yang Lu,[b] Xu-Lin Zhang,[a] Jing Feng,*[a] Qi-Dai Chen[a] and Hong-Bo Sun*[ab]

Received 10th August 2012, Accepted 17th September 2012
DOI: 10.1039/c2jm35394f

Herein, ultrathin crystals of 1,4-bis(4-methylstyryl)benzene (BSB-Me) with excellent mechanical flexibility have been grown by physical vapor transport method and used as active materials in distributed feedback laser devices. In order to maintain the excellent self-waveguide properties of organic single crystals, we adopt a double-layered laser configuration and demonstrate lasing both from one- and two-dimensional distributed feedback. The thin single crystals were further extended onto mechanically bendable poly(ethylene terephthalate) (PET) substrates and presented a proof-of-concept "flexible" organic single-crystal DFB laser. The "flexible" single-crystal laser could be bent with a radius less than 1 cm and recovers after more than 1000 bending cycles.

1. Introduction

Flexibility is one of the most important merits for organic semiconductors compared to their inorganic counterparts, which makes them promising candidates for flexible optoelectronics.[1–10] Low molar mass organic semiconductors in single crystal form exhibit unequalled performances in terms of carrier mobility and device reproducibility in organic electronics with respect to their amorphous counterpart. The long-range order and high chemical purity in crystals make them intrinsically excellent in charge-carrier transport and photonic properties. The recent investigations on collective stimulated emission processes in organic crystals have proven that these materials possess a high gain coefficient, and the electromagnetic field within the crystals shows self-waveguiding properties and well-defined polarization states.[11–17] On the other hand, organic crystals are built from molecules connected by weak intermolecular interactions, which may give rise to the diversities of organic crystal structures (polymorphs and topologies) and variety in photoelectronic properties.[18] The carrier mobility and optical gain in crystals have been significantly enhanced due to improved synthetic methods and design of novel oligomers,[19–25] and it may offer renewed hope for electrically pumped laser action. The dilemma is that highly crystalline order is favorable for high-performance devices, while good flexibility typically originates from microscopic disorder.[26] The organic bulk crystals are generally fragile and delicate, which becomes a great limitation for their applications in flexible devices. On the other hand, single crystals of nanometer size exhibit good flexibility[27–29] and this may provide a chance to use ultrathin film crystalline materials to fabricate high-performance flexible photonic devices.

To achieve lasing, it is crucial to introduce optical feedback for crystals. It is relatively easy to fabricate resonators in thin-film devices, with many approaches already reported. However, it is a challenge to fabricate a microstructure directly in crystals. To introduce distributed feedback (DFB) resonators for organic crystals, researchers have developed a laser interference ablation method to fabricate microstructures in organic single crystals.[30] In this ablation method, Bragg grating structures are written directly into the crystal by a high power laser, so that the crystal material acts as both a DFB resonator and gain medium. Since a high power writing laser is used, it may introduce cracks and photodegration in the crystal during the writing process.[30–32]

To overcome this problem and to maintain the intrinsic properties and characteristics of organic single crystals, it is necessary to fabricate as few microstructures directly in crystals as possible. In this study, we adopted a novel simple fabrication strategy for crystal lasers and demonstrated that it is possible to design and fabricate a "flexible" single-crystalline distributed feedback laser utilizing ultrathin crystals with a thickness of hundreds nanometers. Second order one- and two-dimensional photonic crystal resonators are easily constructed on these thin film crystals. The "flexible" single-crystal laser could be bent with a radius less than 1 cm and recovers after more than 1000 bending cycles.

2. Experiments

Crystal growth and preparation

BSB-Me single crystals were grown from commercially available material (Tokyo Chemical Industry Co., Ltd) in a horizontal physical vapor transport apparatus. No further efforts were made to purify the material. Neutral aluminum oxide and organic materials were mixed uniformly with weight/weight

[a]State Key Laboratory on Integrated Optoelectronics, College of Electronic Science and Engineering, Jilin University, 2699 Qianjin Street, Changchun 130012, China. E-mail: jingfeng@jlu.edu.cn, hbsun@jlu.edu.cn
[b]College of Physics, Jilin University, 119 Jiefang Road, Changchun 130023, China

ratios 5 : 1 through grinding and were subsequently put into a quartz boat. The quartz boat loaded with the mixture was then put into the center of a quartz tube, which was inserted into the high temperature zone of the tube furnace. An initial sublimation temperature of about 270 °C was employed, while the deposition zone temperature was set at 240 °C. High purity nitrogen was used as a carrier and to prevent the organic materials from being oxidized. The morphology is highly dependent on the gas flow; here, the gas flow rate was kept at 200 mL min^{-1}. The single crystals were grown hanged inside the growth tubes.

Optical simulation

Home-generated finite-difference time domain (FDTD) codes were used to calculate the distribution of the electromagnetic field. Firstly, we used the transfer matrix method to obtain the TM-polarized Eigen field distribution in the crystal waveguide, which is set as the input source for the FDTD simulation. Then, the periodic structure is modeled and a 10 000-steps FDTD simulation is performed and $\lambda = 490$ nm.

Device fabrication

The high quality crystals were chosen and laminated on the substrate, on which there is a layer of UV-curable adhesive NOA61 resist (~100 nm thickness). The lamination processes of crystals were performed cautiously to avoid formation of air bubbles between crystal and substrate. The grating structures on top of this crystal layer are fabricated using interference lithography and are written directly into the positive photoresist (S1805). In the experiment, a 266 nm continuous wave (CW) laser on (MBD 266, Coherent) was employed as the coherent interference light source. An electromechanical shutter controls the exposure time. The samples were loaded on the stage and exposed to the pulsed interference pattern. A beam expander was used in the experiment so as to achieve uniform fluence in the central patterned area. After explosion of the 266 nm laser, the photoresist was then developed and grating structures form on the crystal surface.

Lasing characteristics

Lasing characteristics were performed by irradiating the sample with a pulsed laser. The second harmonic generation (~400 nm) of a regenerative amplifier (Spitfire, Spectra Physics, 1 KHz) was used as the pump source. The spot size of the pump laser on the samples was estimated to be about 1 mm in radius. A neutral density filter was used to adjust the excitation intensities. The emitted light was detected by the optical fiber and then dispersed to the spectrometer connected with CCD. The photopumped laser measurements were conducted under atmospheric conditions at room temperature.

3. Results and discussion

3.1. Large-size ultrathin flexible crystalline material

We choose 1,4-bis(4-methylstyryl)benzene (BSB-Me) as the active materials. Fig. 1a shows the chemical structure of BSB-Me and fluorescence photograph of a typical single crystal under the UV light. The edges of the crystal give stronger emission as compared with the body surface, indicating that the self-waveguided emission occurs in the crystals. The spectroscopic properties of BSB-Me crystal are illustrated in the Fig. 1c; there is a strong absorption near 400 nm and the PL spectra is centered around 490 nm. Rapid physical vapor growth conditions enabled single crystals to grow as thin as 200 nm and as large as 0.5 cm × 0.5 cm in size. Interestingly, the grown crystals are nearly transparent and flexible, as captured in Fig. 1b that illustrates a thin crystal naturally "bending" at the tip of a tweezer. No noticeable damage to the crystal occurred after severe bending. The *in situ* manipulation of such an individual crystal gave direct evidence of reversible bending of organic ultrathin film crystals. The crystals with a thickness of hundreds nm have more excellent flexibility and they can be bent and restored under interaction of air flow. This particular attribute enables the high-quality single crystals to conform to curvaceous substrates, thus allowing bending experiments to be conducted. The flexibility in BSB-Me crystals may be attributed to the weak intermolecular interactions in organic crystals, which is different from crystalline inorganic semiconductors. A close analysis of the thin single crystals shows a nearly defect-free surface morphology. The AFM image of the surface morphology of single crystals shows that it has small frequent surface steps. A surface scan over a 10 μm × 10 μm area yielded only one surface step.

3.2. Design and fabrication of crystalline distributed feedback resonators

In order to keep the naturally formed flat surface and maintain the intrinsic properties and characteristics of the single crystals, a double-layered DFB structure was adopted for the crystal lasers,

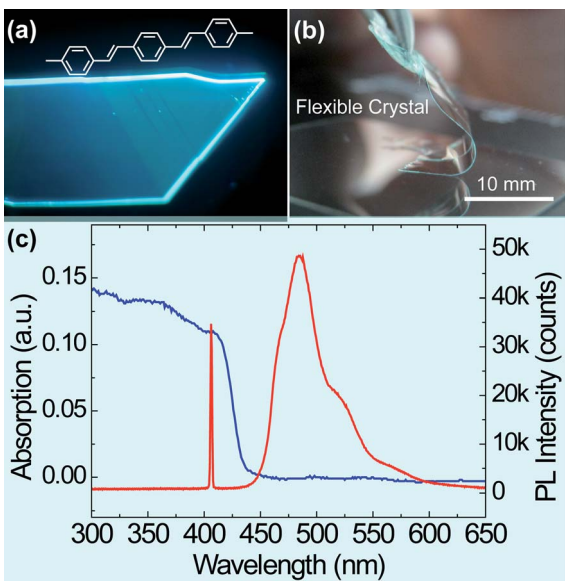

Fig. 1 (a) A fluorescence photograph of BSB-Me crystal under UV light irradiation. Inset: the chemical structure of BSB-Me. (b) A BSB-Me single crystal under the daylight. These thin crystals are nearly transparent and flexible, as captured in the image that shows a thin crystal naturally "bending" by a tweezer. This particular attribute enables the high-quality single crystals to conform to curvaceous substrates, thus allowing bending experiments to be conducted. (c) The absorption (left curve) and the photoluminescence spectra of BSB-Me crystal (right curve).

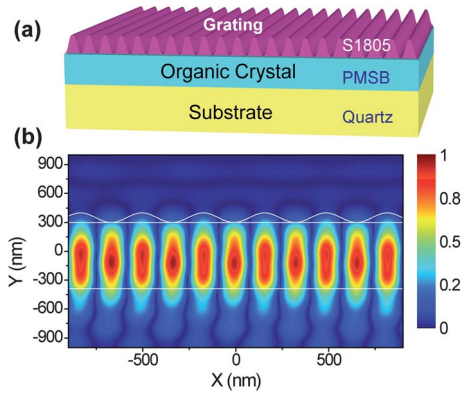

Fig. 2 (a) The design of the crystal distributed feedback waveguide laser. (b) The Eigen modes (electric field energy) of the DFB design with the grating fabricated on top of the continuous crystal waveguide.

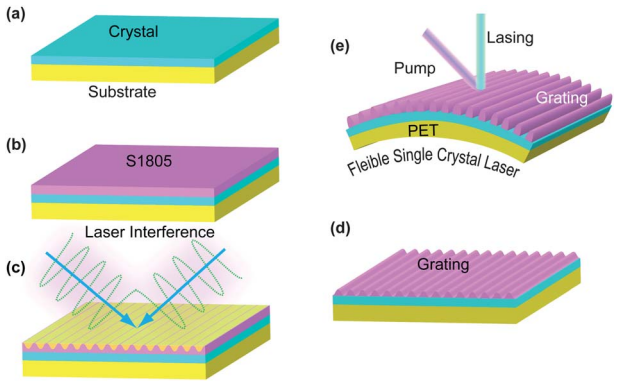

Fig. 3 The fabrication process of the crystal DFB laser. (a) Laminate the grown crystal onto the substrate. (b) Spin-coat the photoresist onto the crystal layer. (c) Laser interference pattern the resist. (d) Development of the photoresist. (e) A schematic illustration of a flexible crystal laser device.

as shown in Fig. 2a. It is composed of a Bragg grating layer and an active waveguide layer of thin crystal. An optical simulation was performed to calculate the field intensity inside the model structure. To introduce efficient feedback, it is important to ensure optical coupling between the crystal waveguide and photoresist diffractive grating. In the simulation, monochromatic light (λ = 490 nm) was injected into the crystal. Theoretical simulation indicates that the field distribution of the Eigen mode is confined almost completely in the active waveguide layer, as shown in Fig. 2b. The light travelled back and forth in the crystal. This implies efficient utilization of the active volume and efficient extraction of the pump energy, as well as oscillation modes. In contrast to the previous work, a non-destructive machining process of the organic crystal is employed in this configuration. It doesn't need to fabricate gratings in crystals. It could keep the naturally formed flat surface and maintain the intrinsic properties and characteristics of the single crystals. It is expected to provide high-quality active waveguide, which favors homogeneous, stable and strong confinement of the oscillation modes in the microcavity formed by the DFB-waveguide mechanism. Moreover, it is much easier to fabricate grating structures in commercial photoresists than in organic

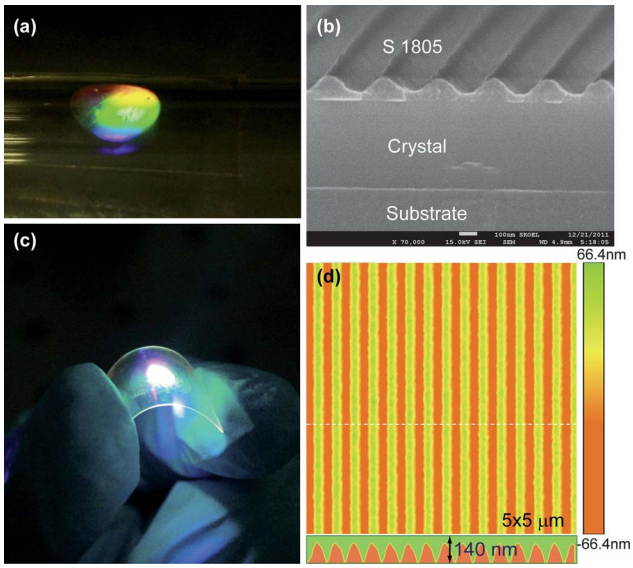

Fig. 4 (a) Iridescence color caused by the diffraction of the fabricated grating could be observed from a sample device. (b) The SEM image of a side view of the device with one-dimensional (1D) grating. (c) A photograph of an experimental flexible single-crystal laser device. UV illumination is used to show the devices fluorescence. (d) AFM images of a one dimensional DFB structures. The period is about 330 nm, the modulated depth is more than 100 nm.

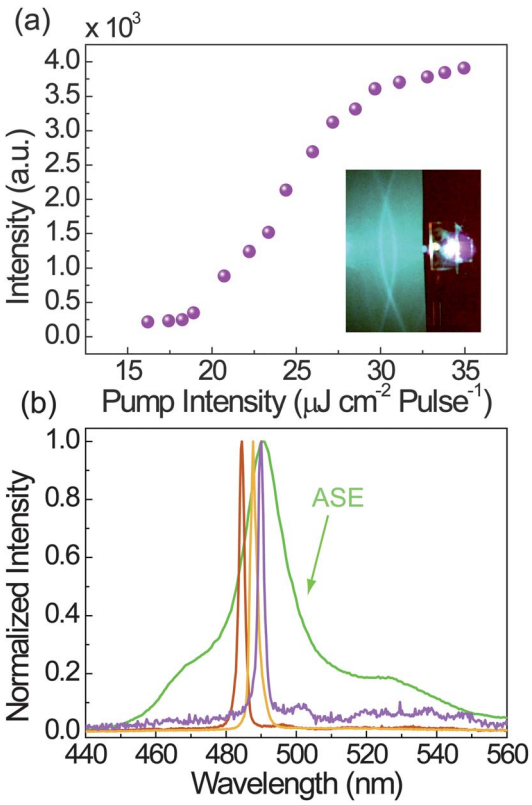

Fig. 5 (a) Output intensity as a function of the pump fluence, indicating a pump threshold of about 18 μJ cm^{-2}. The inset shows photographs of an operating BSB-Me crystal one-dimensional DFB laser. (b) The light-emission spectrum from BSB-ME in the presence of ASE and laser action from three different DFB grating periodicities.

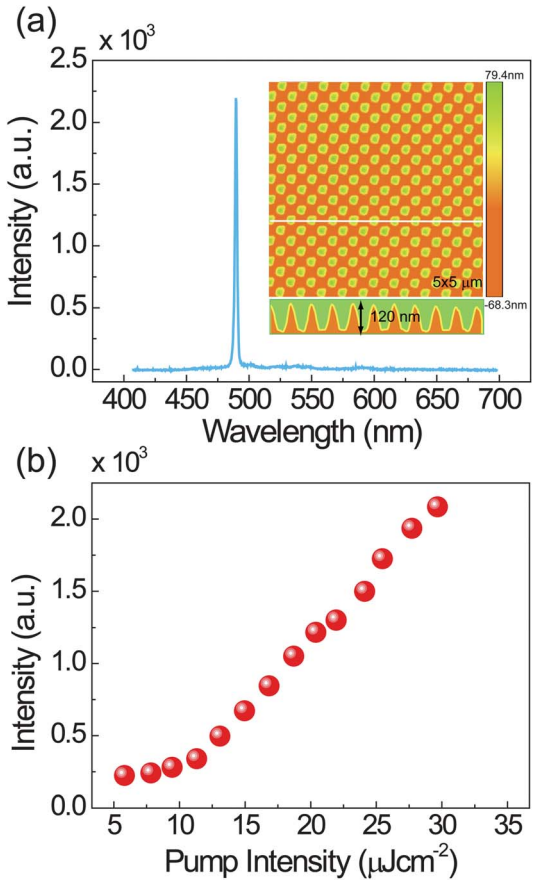

Fig. 6 (a) Laser action from a two-dimensional DFB structure. The inset shows AFM images of two dimensional DFB structures. (b) Output intensity as a function of the pump fluence, indicating a pump threshold of about 10 μJ cm^{-2}.

crystals; the structural parameters of the grating can be controlled and characterized precisely and independently on the species of crystal.

Fig. 3 illustrates the fabrication process of the crystal DFB laser. Firstly, UV-curable adhesive NOA61 resist was spin-coated to form about ~50 nm thick film on the cleaned substrate. Then, the grown thin crystals were transferred from the quartz tube and laminated onto the substrates. The crystals were then adhered to the substrate under UV irradiation and spin-coated with ~140 nm S1805 (Shipley). After that, the prepared samples were exposed to the interference pattern of two-beam laser interference. Here, a 266 nm continuous wave (CW) laser with power 1 W was used and the exposure time was set at 50 ms. The corrugation is ultimately defined after development of the photoresist. Using this holographic exposure technique, highly uniform one-dimensional (1D) sinusoidal intensity profiles can be generated. Two-dimensional (2D) patterns are achieved if the sample is rotated 90° between two subsequent exposures. A "flexible" laser device could be fabricated on mechanically flexible substrates. Poly(ethylene terephthalate) (PET) with a thickness of 0.5 mm was employed as a flexible substrate.

A photograph of a fabricated flexible DFB structure mounted on a glass tube is exhibited in Fig. 4a, where iridescent color caused by the diffraction from the grating region could be clearly observed. The photograph in the inset of Fig. 4c demonstrates the mechanical flexibility of the crystal devices. The cross-section of a one-dimensional DFB laser structure is shown in Fig. 4b. The SEM image confirmed that the double-layered structure was composed of a Bragg grating and a crystal layer as active media. Fig. 4d shows the atomic force microscopy (AFM) images of the one dimensional DFB structures, which have a period of about 330 nm. The modulation depth is approximately 100 nm. The value of the modulation depth is directly related to the thickness of the photoresist film, determined by the spin-coating speed, and exposure time on the resist.

3.3. Lasing performance

The periods of grating structures were selected for second order operation. They were carefully chosen so that feedback could be achieved at wavelengths within the gain region. Laser pulses at 400 nm, second harmonic generation from a Ti:sapphire amplifier, were used as pump light source. The pump pulses are incident onto the sample at an angle of about 20° after being focused by a lens with a focal length of 400 mm. The spot size of the pump laser on the polymer film is estimated to be about 1 mm in radius. Our investigation of the organic single crystals laser begins by examining the performance of thin, single crystals on flat substrates. For a typical sample, the emission intensity of a one-dimensional DFB laser as a function of the pump fluence is depicted in Fig. 5a. A pump threshold of about 18 μJ cm^{-2}, corresponding to a single pulse energy of about 35 nJ was found. It is very similar to the results reported by Namdas.[33] Considering that the S1805 has an absorbance at 400 nm, there is still space for reducing the pump threshold through taking advantage of the resist without absorption at the pump wavelength. To further reduce the lasing threshold and improve the lasing performance is a central issue in future work. The inset of Fig. 5a shows the photograph of the lasing action from one dimensional laser devices. The spectra of the laser emission from three different samples are illustrated in Fig. 5b, along with amplified spontaneous emission from the BSB-Me crystal. The lasing emissions have a bandwidth of about 2 nm at the full width at half maximum (FWHM). In comparison with DFB lasers fabricated by other methods, the line width is relatively wide. It may arise from a relative weak optical coupling between the active crystal waveguide and photoresist diffractive gratings.[29] The wavelength corresponds to the second order Bragg distributed feedback. The spectral position of laser line is determined by the Bragg expression:[34]

$$m\lambda_{\mathrm{Bragg}} = 2n_{\mathrm{eff}}\Lambda \quad (1)$$

where Λ is the periodicity of the grating, m is the order of the diffraction and n_{eff} is the effective refractive index of the waveguide, which is a geometrical average of the refractive indices of the layers of the waveguide and is calculated through a solution of the Helmholtz wave equation for a planar multilayer structure. It should be noted that the period of these three samples are both 330 nm. Since the thickness of the grown crystal is difficult to control, this parameter along with n_{eff} for different devices varies from one to another, and then there is a shift of the laser line.

Two-dimensional (2D) grating patterns could be achieved by using twice-holographic exposure to fabricate a two-dimensional

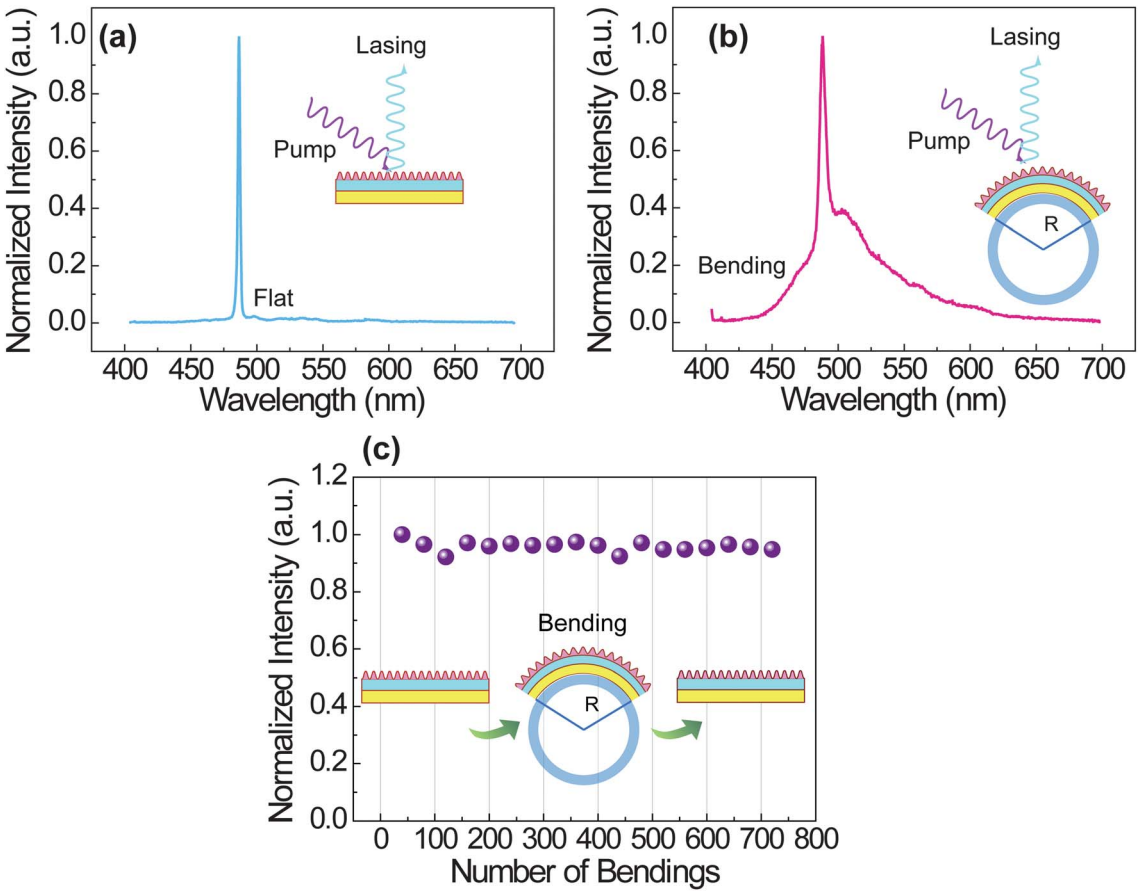

Fig. 7 Measured spectra of the lasing emission at flat (a) and bending state (b). (c) Normalized output intensity as a function of the number of bending cycles. The flexible device can be bent to a radius of less than 1 cm and relaxed to be flat. After more than 800 bending cycles, the intensity shows no evident decrease. The inset shows a schematic illustration of the mechanical stability test of the flexible organic laser devices that was carried out by repeatedly bending the devices with a bending radius of 12.5 mm.

distributed feedback laser. Fig. 6a shows a typical emission spectra with a laser line width of 0.9 nm from a 2D DFB laser. The inset of Fig. 6a illustrates an AFM image of highly uniform 2D crossed grating structures. The dependence of the peak output intensity on the pump pulse energy indicates a laser threshold of about 10 μJ cm^{-2}, which is slightly lower than the value of the 1D structure. This may be attributed to the stronger photon confinement within the guiding gain region provided by the 2D structure.[35]

3.4. Mechanical properties on flexible substrate

We then extended our analysis of thin single crystal lasers onto mechanically flexible substrates to yield conceptual devices that illustrate potential use in practical flexible devices. The bending measurements were performed by attaching the flexible devices onto curved cylinders. The device can be bent to a radius of less than 1 cm and re-released to be flat. The normalized spectra of the lasing emission at flat and bending state ($R \sim 1.25$ cm) are shown in the Fig. 7a and b, respectively. Remarkably, the bended device exhibits a broadened spectra and less lasing efficiency during the bending state, which may arise from the bending loss. A mechanical stability test of the flexible organic laser devices was carried out by repeatedly bending the devices with a bending radius of 12.5 mm. Interestingly, the lasing intensity and the spectra recover after releasing the flexible substrate from a bending state. The normalized output intensity as a function of the number of bending cycles is shown in Fig. 7c. After more than 800 bending cycles, the lasing shows no evident decease in intensity. A noticeable fracture in the crystal after the bending test was excluded, since the fracture may become a scattering centre of light and reduce lasing intensity. These results evidently demonstrate the durability to flexing and imply that lasers fabricated from BSB-Me thin single crystals may have potential use in applications where ruggedness and mechanical flexibility are a requirement.

The lasing lifetime performance, when operating above the lasing threshold at room temperature and in an ambient atmosphere, was further tested. This has been studied by recording the DFB intensity as a function of number of pump pulses, at constant pump energy above the threshold at the same spot of the film. Fig. 8a shows the evolution of the laser emission spectrum when pumped continuously for 2.0×10^7 pulses above the threshold. The peak intensity evolution is plotted in Fig. 8b. The device lifetime, defined as the photo-stability 1/*e*-life ($\tau_{1/e}$), *i.e.*, the number of pump pulses at which the emitted laser intensity decays to 1/*e* of its maximum value, exceeds 1.3×10^7 pulses. The grating layer on the top may help to improve the stability, which

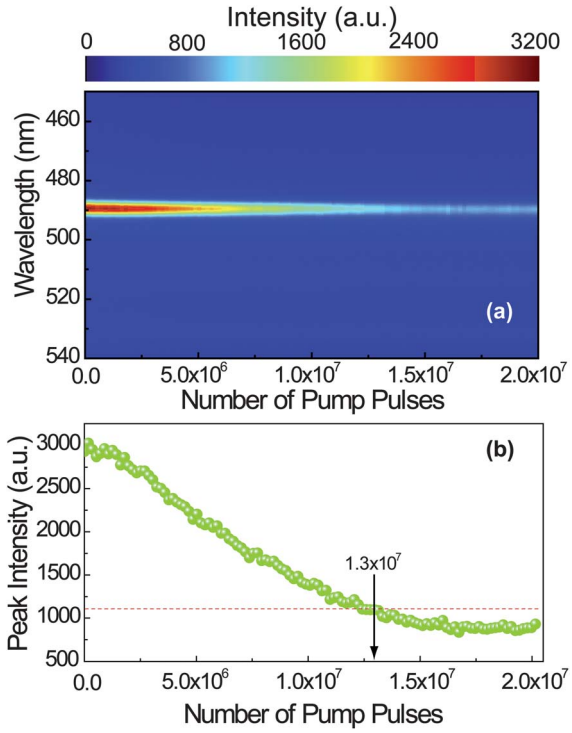

Fig. 8 (a) A photostability test for an operating 1D DFB crystal laser, (a) spectral evolution and (b) peak intensity as a function of the number of pump pulses.

could work as an encapsulating layer protecting the underneath of the BSB-Me crystal from photo-degradation.

4. Conclusions

In summary, we have reported flexible organic crystal distributed feedback laser based on the BSB-Me thin organic crystals. The two-layered structures enable us to construct the distributed feedback laser facilely and avoid ablation of the organic crystal. These devices function well after mild mechanical tensile strain. These results are promising in view of developing innovative low-cost, flexible and photostable crystal lasers and, therefore, open up a large number of novel applications.

Acknowledgements

The authors would like to acknowledge the Natural Science Foundation, China (NSFC) under Grants no. 90923037, 10904049, 61137001 and 61127010 for support.

References

1 S. C. B. Mannsfeld, B. C. K. Tee, R. M. Stoltenberg, C. V. H. H. Chen, S. Barman, B. V. O. Muir, A. N. Sokolov, C. Reese and Z. Bao, *Nat. Mater.*, 2010, **9**, 859–864.
2 J. F. Fang, P. Matyba and L. Edman, *Adv. Funct. Mater.*, 2009, **19**, 2671–2676.
3 A. L. Briseno, R. J. Tseng, M. M. Ling, E. H. L. Falcao, Y. Yang, F. Wudl and Z. N. Bao, *Adv. Mater.*, 2006, **18**, 2320–2324.
4 S. J. Kim and J. S. Lee, *Nano Lett.*, 2010, **10**, 2884–2890.
5 J. A. Rogers, Z. Bao, K. Baldwin, A. Dodabalapur, B. Crone, V. R. Raju, V. Kuck, H. Katz, K. Amundson, J. Ewing and P. Drzaic, *Proc. Natl. Acad. Sci. U. S. A.*, 2001, **98**, 4835–4840.
6 J. Yoon, W. Lee and E. L. Thomas, *Nano Lett.*, 2006, **6**, 2211–2214.
7 C. Kallinger, M. Hilmer, A. Haugeneder, M. Perner, W. Spirkl, U. Lemmer, J. Feldmann, U. Scherf, K. Müllen and A. Gombert, *Adv. Mater.*, 1998, **10**, 920–923.
8 M. Anni, *Appl. Phys. Lett.*, 2011, **98**, 253304.
9 F. Scotognella, A. Monguzzi, F. Meinardi and R. Tubino, *Phys. Chem. Chem. Phys.*, 2010, **12**, 337–340.
10 J. Herrnsdorf, B. Guilhabert, Y. Chen, A. L. Kanibolotsky, A. R. Mackintosh, R. A. Pethrick, P. J. Skabara, E. Gu, N. Laurand and M. D. Dawson, *Opt. Express*, 2010, **18**, 25535–25545.
11 D. Fichou, S. Delysse and J. M. Nunzi, *Adv. Mater.*, 1997, **9**, 1178–1181.
12 H. Yanagi and T. Morikawa, *Appl. Phys. Lett.*, 1999, **75**, 187–189.
13 H. Yanagi, T. Ohara and T. Morikawa, *Adv. Mater.*, 2001, **13**, 1452–1455.
14 H. Xia, J. Yang, H. H. Fang, Q. D. Chen, H. Y. Wang, X. Q. Yu, Y. G. Ma, M. H. Jiang and H. B. Sun, *ChemPhysChem*, 2010, **11**, 1871–1875.
15 Q. L. Bao, B. M. Goh, B. Yan, T. Yu, Z. A. Shen and K. P. Loh, *Adv. Mater.*, 2010, **22**, 3661–3666.
16 W. J. Xie, Y. P. Li, F. Li, F. Z. Shen and Y. G. Ma, *Appl. Phys. Lett.*, 2007, **90**, 141110.
17 M. Polo, A. Camposeo, S. Tavazzi, L. Raimondo, P. Spearman, A. Papagni, R. Cingolani and D. Pisignano, *Appl. Phys. Lett.*, 2008, **92**, 083311.
18 Z. Q. Xie, L. L. Liu, B. Yang, G. D. Yang, L. Ye, M. Li and Y. G. Ma, *Cryst. Growth Des.*, 2005, **5**, 1959–1964.
19 Z. Q. Xie, B. Yang, F. Li, G. Cheng, L. L. Liu, G. D. Yang, H. Xu, L. Ye, M. Hanif, S. Y. Liu, D. G. Ma and Y. G. Ma, *J. Am. Chem. Soc.*, 2005, **127**, 14152–14153.
20 H. Wang, F. Li, I. Ravia, B. R. Gao, Y. P. Li, V. Medvedev, H. B. Sun, N. Tessler and Y. G. Ma, *Adv. Funct. Mater.*, 2011, **21**, 3770–3777.
21 S. Park, O. H. Kwon, S. Kim, S. Park, M. G. Choi, M. Cha, S. Y. Park and D. J. Jang, *J. Am. Chem. Soc.*, 2005, **127**, 10070–10074.
22 H. H. Fang, Q. D. Chen, J. Yang, H. Xia, B. R. Gao, J. Feng, Y. G. Ma and H. B. Sun, *J. Phys. Chem. C*, 2010, **114**, 11958–11961.
23 J. Yang, H. H. Fang, R. Ding, S. Y. Lu, Y. L. Zhang, Q. D. Chen and H. B. Sun, *J. Phys. Chem. C*, 2011, **115**, 9171–9175.
24 H. H. Fang, Q. D. Chen, J. Yang, L. Wang, Y. Jiang, H. Xia, J. Feng, Y. G. Ma, H. Y. Wang and H. B. Sun, *Appl. Phys. Lett.*, 2010, **96**, 103508.
25 R. Kabe, H. Nakanotani, T. Sakanoue, M. Yahiro and C. Adachi, *Adv. Mater.*, 2009, **21**, 4034–4038.
26 H. Sirringhaus, P. J. Brown, R. H. Friend, M. M. Nielsen, K. Bechgaard, B. M. W. Langeveld-Voss, A. J. H. Spiering, R. A. J. Janssen, E. W. Meijer, P. Herwig and D. M. de Leeuw, *Nature*, 1999, **401**, 685–688.
27 Q. X. Tang, Y. H. Tong, Y. M. Zheng, Y. D. He, Y. J. Zhang, H. L. Dong, W. P. Hu, T. Hassenkam and T. Bjornholm, *Small*, 2011, **7**, 189–193.
28 A. L. Briseno, S. C. B. Mannsfeld, X. M. Lu, Y. J. Xiong, S. A. Jenekhe, Z. N. Bao and Y. N. Xia, *Nano Lett.*, 2007, **7**, 668–675.
29 Y. Wakayama, R. Hayakawa, T. Chikyow, S. Machida, T. Nakayama, S. Egger, D. G. de Oteyza, H. Dosch and K. Kobayashi, *Nano Lett.*, 2008, **8**, 3273–3277.
30 H. H. Fang, R. Ding, S. Y. Lu, J. Yang, X. L. Zhang, R. Yang, J. Feng, Q. D. Chen, J. F. Song and H. B. Sun, *Adv. Funct. Mater.*, 2011, **22**, 33.
31 T. R. Zhai, X. P. Zhang, Z. G. Pang and F. Dou, *Adv. Mater.*, 2011, **23**, 1860–1864.
32 H. H. Fang, R. Ding, S. Y. Lu, L. Wang, J. Feng, Q. D. Chen and H. B. Sun, *Opt. Lett.*, 2012, **37**, 686–688.
33 E. B. Namdas, M. Tong, P. Ledochowitsch, S. R. Mednick, J. D. Yuen, D. Moses and A. J. Heeger, *Adv. Mater.*, 2009, **21**, 799–802.
34 I. D. W. Samuel and G. A. Turnbull, *Chem. Rev.*, 2007, **107**, 1272–1295.
35 G. Heliotis, R. D. Xia, G. A. Turnbull, P. Andrew, W. L. Barnes, I. D. W. Samuel and D. D. C. Bradley, *Adv. Funct. Mater.*, 2004, **14**, 91–97.